Relaxational dynamics of smectic phases on a curved substrate

Leopoldo R. Gómez* and Daniel A. Vega†
Department of Physics, CONICET–Universidad Nacional del Sur, Av. L.N. Além 1253 (8000) Bahía Blanca, Argentina
(Received 14 August 2008; published 3 March 2009)

We study the dynamics of pattern formation of two-dimensional smectic systems constrained to lie on a substrate with sinusoidal topography. We observe a coupling between defects and geometry that induces the preferential location of positive (negative) defects onto regions with positive (negative) Gaussian curvature. For the curvatures studied here we observe unbinding and self-organization of disclination pairs. The local orientation of the pattern and the location of topological defects can be accurately controlled with the curvature of the underlying substrate. Thus, long-range interactions arising from the geometry of the substrate lead to ordered patterns with potential applications to nanotechnology.

DOI: 10.1103/PhysRevE.79.031701 PACS number(s): 61.30.Hn, 68.15.+e, 02.40.−k

Striped phases are present in a wide variety of physical systems such as ferrimagnetic films with dipolar interactions, Langmuir monolayers, Rayleigh-Bénard convection cells, liquid crystals, and symmetric block copolymers [1,2]. Equilibrium and nonequilibrium features of two-dimensional (2D) striped phases have been intensively studied in the last three decades. In these systems, most of the attention has been focused on the role of topological defects in the dynamics of phase transitions [3].

In the last years, the studies of self-assembly in 2D systems have also been driven by the possible applications to nanotechnology [4]. For example, thin-film patterns of block copolymers have been used as nanolithographic masks for pattern transfer [5]. One of the main difficulties associated to these systems is the lack of long-range order due to the presence of unavoidable topological defects [6]. For striped patterns it was shown that correlation lengths grow slowly with the annealing time during thermal treatments, mainly due to the annihilation of multipoles of disclinations (orientational topological defects) [6]. Slow kinetics of ordering has also been observed in systems with hexagonal symmetry [7,8]. Since most of the nanotechnological applications of self-assembled systems require well ordered patterns, different strategies have been employed to induce long-range order [9].

Recently, there has been an increasing interest in the study of 2D modulated phases on nonflat surfaces [10–18]. One of the main differences between planar and curved 2D modulated phases is the nature of topological defects. The curvature of the substrate can impose a topological requirement involving defects in the equilibrium state. This topological requirement is given by the Gauss-Bonnet theorem which relates the integral of the Gaussian curvature with the total disclination charge [10–18].

From the first insights, most of the studies have considered 2D striped phases on spheres. By using the Frank free energy in the one constant approximation, Lubensky and Prost [10] showed that in nematic phases constrained to lie on spheres the fundamental state is given by four +1/2 disclinations located at the vertex of a tetrahedron (baseball configuration). It was pointed out that this particular arrangement of defects can be functionalized to obtain divalent or tetravalent spheres [19,20]. In the case of smectic phases on spheres, defect configurations including hedgehog, spirals, and quasibaseball have been identified [11] and recently observed by self-consistent calculations of lamellar forming block copolymers [12].

In this work we investigate the kinetics of ordering of a 2D smectic phase constrained to lie on a curved sinusoidal substrate. Although in our system there is no topological requirement for the existence of defects, since the energy of a defect-free state grows as the curvature of the substrate is increased [10], it is expected that the system relaxes the strain field energy by locating defects on preferential surface sites.

Here we consider the process of pattern formation of a striped phase described by the following free-energy functional [2,21]:

$$F = \int d^2r\sqrt{g}\left[U(\psi) + \frac{D}{2} g^{\alpha\beta}\partial_\alpha\psi(\mathbf{r})\partial_\beta\psi(\mathbf{r}) \right] - \frac{b}{2}\int\int d^2r d^2r' \sqrt{g}\sqrt{g'} G(\mathbf{r}-\mathbf{r}')\psi(\mathbf{r})\psi(\mathbf{r}'), \quad (1)$$

where ψ describe the order parameter field, $U(\psi)=-\tau\psi^2+u\psi^4$ is the typical double well with two minima, D is related to the penalization to form interfaces, g is the determinant of the metric $g_{\alpha\beta}$ of the curved substrate, and $G(\mathbf{r}-\mathbf{r}')$ is a Green's function which takes into account the competing long-range interactions.

Recently, Santangelo *et al.* [13] have argued that the extrinsic curvature may be an important factor in determining the pattern configuration of columnar phases. In that study, the columnar phases were obtained with a 0.3 μm thick film of a cylinder forming block copolymer deposited on a curved substrate. The experiments image the top layer of a film roughly ten layers thick [top layer of a three-dimensional (3D) array of hexagonally packed cylinders]. It has been argued that due to the coupling with the extrinsic curvature, a boundarylike term aligns the columns at the regions where the Gaussian curvature of the substrate changes the sign.

*lgomez@uns.edu.ar
†dvega@criba.edu.ar

 ©2009 The American Physical Society

However, how the underlying layers (which necessarily contains topological defects and strains) couple to the two-dimensional geometry of the topmost layer and how it affects the equilibrium configuration is still an open question [13].

Note that Eq. (1) does not include any coupling with the extrinsic curvature. However, since experimentally the effect of the extrinsic curvature could be strongly reduced (for example by using thin films of symmetric block copolymers), Eq. (1) provides a good approximation to describe the properties of experimental two-dimensional smectic systems. In addition, note also that Eq. (1) can be extended to take into account the coupling with the extrinsic curvature by considering, for example, a monolayer of cylinders rather that a strictly two-dimensional system.

The dynamic evolution of a smectic system quenched into the spinodal region of the phase diagram can be obtained through the following relaxational equation:

$$\frac{\partial \psi}{\partial t} = M\nabla^2_{\mathrm{LB}}\left\{\frac{\delta F}{\delta \psi}\right\} + \eta(\mathbf{r},t). \tag{2}$$

Here M is a phenomenological mobility coefficient, η is a white random noise term to take into account thermal fluctuations [7], and $\nabla^2_{\mathrm{LB}}=\frac{1}{\sqrt{g}}\frac{\partial}{\partial x^\alpha}(\sqrt{g}g^{\alpha\beta}\frac{\partial}{\partial x^\beta})$ is the Laplace-Beltrami operator, which reduces to the classical Laplacian for flat systems [22]. Equation (2) leads to spinodal decomposition for $\tau > \tau_s$, where $\tau_s = 2\sqrt{Db}$ is the critical temperature. In the case of 2D planar systems this coarse grained model has probed to be a remarkable tool to study dynamical and equilibrium features of 2D modulated phases [2,7,8].

Here we numerically solve Eq. (2) on a sinusoidal geometry by using a finite difference forward in time center space scheme on a 512×512 grid. The dynamics is studied for a substrate of square symmetry described by: $\mathbf{R}=x\mathbf{i}+y\mathbf{j}+f(x,y)\mathbf{k}$, with $f(x,y)=A\cos(2\pi x/L)\cos(2\pi y/L)$ [see Fig. 1(a)]. Here $\mathbf{i}$, $\mathbf{j}$, and $\mathbf{k}$ are the basis Cartesian vectors, $L\sim 37\pi/k_0$, $A\sim 16\pi/k_0$, $k_0=0.45\sim(b/D)^{1/4}$ is the local wave vector amplitude of the striped pattern (Fig. 1) and $L=256$ is the side length of the 2D projection of the surface onto the x-y plane. Then, here the substrate deformation [18] becomes $A2\pi/L\sim 0.86\pi$. In order to study the relaxational dynamics of an initial homogeneous system quenched into the unstable region of the phase diagram, we solve Eq. (2) in a square cell of area L^2 starting from a random initial condition [7,8].

Figures 1(b) and 1(c) show the dynamics of pattern formation for a system deeply quenched into the unstable region ($\tau_s/\tau=0.6$). Figure 1(b) shows the pattern configuration of the system at early times. As a consequence of the competing interactions, we observe a fast length scale selectivity. However, differently from the patterns observed in flat systems, where the early domains are roughly circular [7], here the curvature of the substrate induces a preferential alignment of the domains, which becomes distorted along the parallels of the substrate (z=constant). Although the orientation of the domains is relatively well defined at early times, there is a poor connectivity and a high density of uniformly distributed defects.

Similarly to planar systems, as time proceeds, the degree of order increases led by an increment of domain connectivity and the further annihilation of dislocations and multipoles of $\pm 1/2$ disclinations [6]. The intermediate stage of ordering clearly shows the coupling between curvature and stripe orientation [Fig. 1(c)]. In Figs. 1(c) and 1(d) we have included a few representative geodesic lines to show the interrelationship between stripe orientation and geometry. We can observe that in order to minimize the compressional free energy there is a tendency of the normals to the stripes to follow geodesic lines, in agreement with theoretical predictions [13]. However, packing effects can be quite important in determining distribution of topological defects in systems with strong length scale selectivity [12]. These packing effects can be clearly observed in Fig. 1(b), where the free energy in nearly flat regions is relaxed via the unbinding of dislocations.

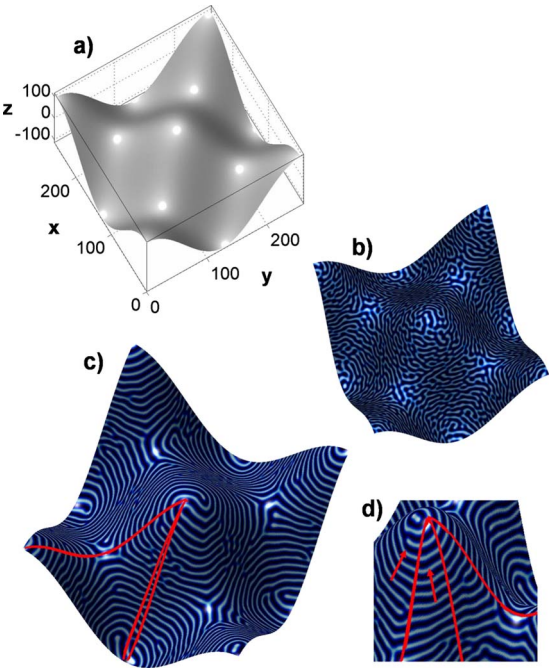

FIG. 1. (Color online) (a) Three-dimensional view of the sinusoidal substrate defined by $\mathbf{R}(x,y)$. The side length of the 2D projection of the surface onto the x-y plane is L. Panels (b) and (c) show the pattern configurations at early and intermediate times, respectively. Panel (d) shows the late time configuration of the smectic pattern on a bump. Red (gray) lines indicate representative geodesics and the arrows the normals to the stripes.

Figure 2 shows the temporal evolution of the number dislocations (N_d). At early times, the decrease in N_d is produced by the increase in the connectivity between near neighbor stripes. Typically, the connectivity between stripes increases by the diffusion of dislocations on distances of order k_0^{-1}. At intermediate times, the further annihilation of dislocations is given by a combination of the glide and climb mechanisms. Here we found that the number of dislocations decreases as $N_d\sim t^{-0.33}$. This slow dynamics of dislocation annihilation is very close to that found experimentally in planar systems [6].

In order to emphasize the relationship between defects and curvature, in Figs. 3(a) and 3(b) we show a x-y projection of a superposition of the Gaussian curvature with the striped pattern. The Gaussian curvature, K, defined as the

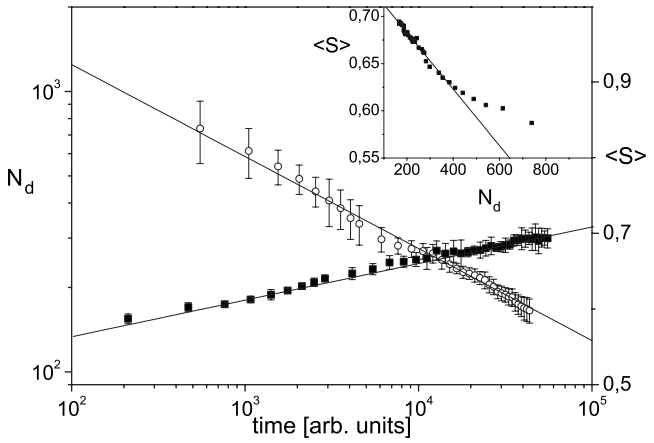

FIG. 2. Number of dislocations N_d (circles) and orientational order parameter $\langle S \rangle$ (squares) as a function of time. The lines correspond to the power law and logarithmic fits, respectively. Inset: $\langle S \rangle$ vs N_d (symbols) and linear fit for the late stage of relaxation.

product of the two principal curvatures, is the intrinsic curvature of the substrate [22]. It is positive in crest and valleys, negative in saddles, and zero in planar regions [Fig. 3(c)] [23].

From this figure it can be easily observed that the cores of most of the disclinations are located on zones of high Gaussian curvature, indicating the strong coupling between topological defects and curvature. It is also clear that positive (negative) disclinations are preferentially located onto regions of positive (negative) curvature. The preferential location of the defects according to the local curvature is in good agreement with the theoretical predictions for the equilibrium properties of liquid crystal phases on curved surfaces [14]. Dislocations are also observed to have preferential orientations, mainly dictated by the constraint of equally spaced stripes.

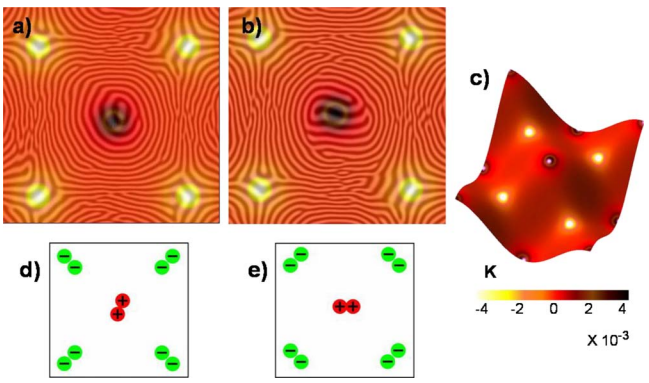

FIG. 3. (Color online) [(a) and (b)] 2D projection of the pattern onto the x-y plane overlapped by the Gaussian curvature of the substrate [panel (c)]. The side length of the 2D projection of the pattern onto the x-y plane is L. (c) 3D view of the Gaussian curvature of the substrate. Color (gray) code indicated on the bottom. [(d) and (e)] Schematic representation of the two arrays of disclinations observed in panels (a) and (b), respectively. These arrays of disclinations are favored energetically by the presence of long-range interactions.

In the regions with the highest curvature we observe arrangements of disclinations rarely found in planar systems [1,6]. While pairs of 1/2 disclinations of the same sign repeal each other in planar systems, here these configurations are stabilized by the curvature of the substrate. For the geometry studied here we observe that the average distance between the disclinations located in the regions of the highest curvature is about $3/k_0$. This distance should be strongly affected by curvature and packing effects, such that binding-unbinding transitions can be expected for other curvatures. Differently from hexagonal systems where the free energy can be relaxed by grain boundary scars [15–18], here we found that the distance between near neighbor disclinations can vary to screen the curvature.

We note that the pairs of $-1/2$ disclinations around saddle points could be locally arranged in two different low-energy configurations. These configurations can be expected to be equally energetic in the absence of long-range interactions. However, Figs. 3(a) and 3(b) show that the orientation of the $-1/2$ pairs of disclinations is not randomly distributed between these two low-energy states. The four negative pairs are located parallel or perpendicular to the four geodesic lines connecting each pair of nearest-neighbor bumps or valleys [compare Figs. 3(a) and 3(b) with the schematic representations of the arrays of disclinations of Figs. 3(d) and 3(e)]. Although the unbinding of $+1/2$ disclinations can be also observed in Fig. 3, it is more difficult to establish the correlation between the local orientation of the pair and the geometry of the substrate.

In general, the free-energy functional for a 2D texture embedded in an arbitrary frozen surface contains only splay and bend terms. In our case, the fixed layer spacing dictates that bend is more energetically costly than splay, forcing $K_3 \gg K_1$ (K_1 and K_3 being the splay and bend constants, respectively). For example, in block copolymer thin films with smectic symmetry it has been found that $K_3/K_1 \sim 40$ [24]. In what follows and for simplicity, we compare our numerical results with a particular solution (pure splay configuration) of the Euler-Lagrange equation associated to the Frank free energy in the one constant approximation [10], [19]. In the one constant approximation, the Frank free energy takes the form $F_F = K_1 \int d^2 r \sqrt{g} [\partial_\alpha m^\beta + \Gamma^\beta_{\alpha\gamma} m^\gamma]^2$, where $\mathbf{m}$ is the normal field of the pattern and Γ^α_γ are connection coefficients associated with the parallel transport of $\mathbf{m}$. This free energy can be written in terms of the local orientation of the normal field of the stripes $\theta(\mathbf{r})$ respect to a basis $\mathbf{e}_1$, $\mathbf{e}_2$ of the tangent plane of the surface (where $\mathbf{m}$ is decomposed as $\mathbf{m} = \cos\theta \mathbf{e}_1 + \sin\theta \mathbf{e}_2$). Then, $F_F = K_1 \int d^2 r \sqrt{g} g^{\alpha\beta} (\partial_\alpha \theta - A_\alpha)(\partial_\beta \theta - A_\beta)$, where $A_\alpha = \mathbf{e}_1 \cdot \partial_\alpha \mathbf{e}_2$ is a connection that compensates the rotation of the basis vectors. The equilibrium configuration is obtained through the associated Euler-Lagrange equation $\nabla^2_{\mathrm{LB}} \theta_0 + \partial_\alpha A_\alpha + \Gamma^\gamma_{\alpha\alpha} A_\gamma = 0$ [10].

For the sinusoidal surface we can choose the basis vectors of the tangent plane as $\mathbf{e}_1 = f_x \mathbf{i} + f_y \mathbf{j} + (f_x^2 + fy^2)\mathbf{k}$, $\mathbf{e}_2 = f_y \mathbf{i} - f_x \mathbf{j}$. We found that a simple pure splay solution satisfying the Euler-Lagrange equation for our problem is given by $\mathbf{m}$ parallel to $\mathbf{e}_1$ throughout the surface.

Figure 4(a) shows the projection of the local orientation $\theta_0(\mathbf{r})$ onto the x-y plane [$\theta_0(\mathbf{r}) = \tan^{-1}(\mathbf{e}_1 \cdot \mathbf{j} / \mathbf{e}_1 \cdot \mathbf{i})$]. We may note that $\theta_0(\mathbf{r})$ rotates an angle of 2π around the bumps and

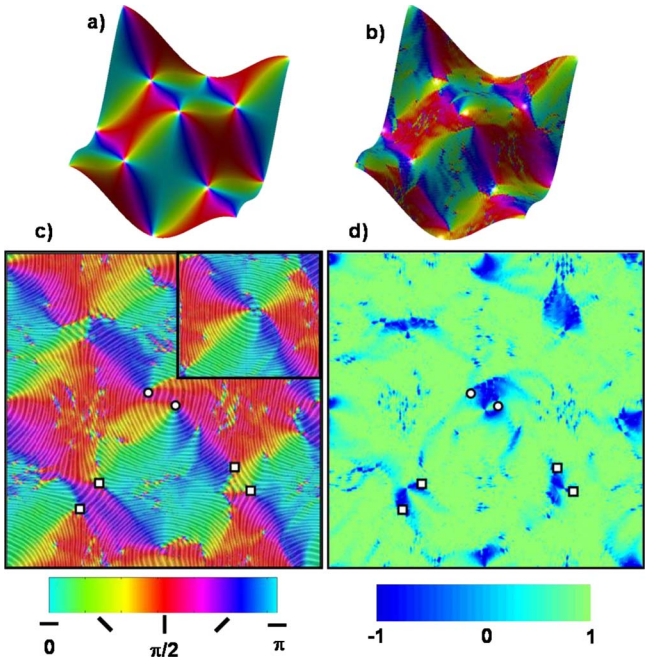

FIG. 4. (Color online) 3D views of (a) $\theta_0(\mathbf{r})$ and (b) $\theta(\mathbf{r})$. (c) 2D projection of the pattern onto the x-y plane overlapped by the local orientation of the stripes. The inset shows $\theta(\mathbf{r})$ on a bump and the bottom of this figure indicates the color (gray) code employed to identify the local orientation. (d) 2D projection of the order parameter S onto the x-y plane at long times. The white squares and circles indicate negative and positive disclinations, respectively. Color (gray) code indicated at the bottom. Here the side length of the 2D projections is L.

valleys, and -2π around the saddles, making these points good candidates to locate disclinations. In order to compare this simple splay pure solution for $\theta_0(\mathbf{r})$ with the late configuration obtained by the simulations, we determine the local orientation of the stripes $\theta(\mathbf{r})$ by the gradient method described elsewhere [6].

The local orientation of the striped pattern is shown in Figs. 4(b) and 4(c). A by eye comparison between $\theta_0(\mathbf{r})$ and the actual pattern [Fig. 4(a) vs Figs. 4(b) and 4(c)] indicates that this solution provides a reasonably good description for the local orientation. Although $\theta_0(\mathbf{r})$ cannot describe adequately the real orientation of the stripes, mainly due to the unbinding of defects (see Figs. 3 and 4), when the distance between pairs of disclinations is small, such as in the inset of Fig. 4(c), the mismatch between both orientational fields becomes small.

A quantitative comparison between the local orientation of the stripes and $\theta_0(\mathbf{r})$ can be obtained by defining an orientational order parameter as $S=\cos(2\Delta\theta)$, where $\Delta\theta$ is the difference between $\theta(\mathbf{r})$ and $\theta_0(\mathbf{r})$. Note that $S=1$ for perfect alignment in the direction dictated $\theta_0(\mathbf{r})$ and $S=0$ for a random orientation. Figure 4(d) shows the map of S onto the surface. Note the excellent agreement between both orientational fields, except at the regions where there is unbinding of disclinations.

In Fig. 2 we show the time dependence of the average of the order parameter ($\langle S\rangle$). Here we found that $\langle S\rangle$ grows roughly logarithmically on time [25]. As compared with planar systems where the dynamics is controlled by the annihilation of multipoles of disclinations (density of disclinations $\sim t^{-1/2}$) [6], here the coupling between defects and geometry leads to a dynamics clearly slower.

Experimental results on shear aligned sphere forming block copolymers deposited onto flat substrates indicate that $\langle S\rangle$ decreases linearly with the number of dislocations [26]. In this case, it has been observed that each dislocation destroys the orientational order in an area of order $1/k_0^2$. In the inset of Fig. 2 we have also included a plot of $\langle S\rangle$ vs N_d. Although here we also found $\langle S\rangle \sim N_d$ at long times, where the density of dislocations is relatively small, at early times the dynamics departs from linearity since the domains are strongly distorted in the direction dictated by the curvature.

In summary, we have studied the influence of the curvature of the substrate on the kinetics of ordering of a pattern with smectic symmetry. We have demonstrated that the orientation of the pattern and the location of topological defects are established at the very early stage of phase separation. This open the possibility of a robust mechanism for an accurate control of smectic textures with potential applications to nanotechnology. For example, curved substrates could be used to accurately control the density and location of defects in thin films of block copolymers. In this sense, the existence of disclinations in the regions of high curvature would allow the creation of novel materials with chemical linkers or biomolecules strands anchored at the core of the defects [20].

This work was supported by the Universidad Nacional del Sur (UNS), the National Research Council of Argentina (CONICET), the National Agency of Scientific and Technique Promotion (ANPCyT), and the USAMI program through the National Science Foundation and Princeton University. The authors are grateful to Richard Register for helpful discussions.

[1] C. Bowman and A. C. Newell, Rev. Mod. Phys. **70**, 289 (1998).
[2] M. Seul and D. Andelman, Science **267**, 476 (1995).
[3] D. R. Nelson, *Defects and Geometry in Condensed Matter Physics* (Cambridge University Press, Cambridge, 2002).
[4] R. A. Segalman, Mater. Sci. Eng., R. **48**, 191 (2005).
[5] M. Park, C. Harrison, P. M. Chaikin, R. A. Register, and D. H. Adamson, Science **276**, 1401 (1997).
[6] C. K. Harrison, D. H. Adamson, Z. Cheng, J. M. Sebastian, S. Sethuraman, D. A. Huse, R. A. Register, and P. M. Chaikin, Science **290**, 1558 (2000).
[7] D. A. Vega, C. K. Harrison, D. E. Angelescu, M. L. Trawick, D. A. Huse, P. M. Chaikin, and R. A. Register, Phys. Rev. E **71**, 061803 (2005).

[8] L. R. Gómez, E. M. Vallés, and D. A. Vega, Phys. Rev. Lett. **97**, 188302 (2006).
[9] S. B. Darling, Prog. Polym. Sci. **32**, 1152 (2007).
[10] T. C. Lubensky and J. Prost, J. Phys. II **2**, 371 (1992).
[11] C. Blanc and M. Kleman, Eur. Phys. J. E **4**, 241 (2001).
[12] T. L. Chantawansri, A. W. Bosse, A. Hexemer, H. D. Ceniceros, C. J. García-Cervera, E. J. Kramer, and G. H. Fredrickson, Phys. Rev. E **75**, 031802 (2007).
[13] C. D. Santangelo, V. Vitelli, R. D. Kamien, and D. R. Nelson, Phys. Rev. Lett. **99**, 017801 (2007).
[14] V. Vitelli and A. M. Turner, Phys. Rev. Lett. **93**, 215301 (2004).
[15] A. R. Bausch, M. J. Bowick, A. Cacciuto, A. D. Dinsmore, M. F. Hsu, D. R. Nelson, M. G. Nikolaides, A. Travesset, and D. A. Weitz, Science **299**, 1716 (2003).
[16] M. J. Bowick, A. Cacciuto, D. R. Nelson, and A. Travesset, Phys. Rev. B **73**, 024115 (2006).
[17] M. J. Bowick, L. Giomi, H. Shin, and C. K. Thomas, Phys. Rev. E **77**, 021602 (2008).
[18] A. Hexemer, V. Vitelli, E. J. Kramer, and G. H. Fredrickson, Phys. Rev. E **76**, 051604 (2007).
[19] D. R. Nelson, Nano Lett. **2**, 1125 (2002).
[20] G. A. DeVries, M. Brummbauer, Y. Hu, A. M. Jackson, B. Long, B. T. Neltner, O. Uzun, B. H. Wunsch, and F. Stellacci, Science **315**, 358 (2007).
[21] T. Ohta and K. Kawasaki, Macromolecules **19**, 2621 (1986).
[22] B. O'Neill, *Elementary Differential Geometry* (Academic, New York, 1997).
[23] It should be noted that here the local wave vector amplitude is constant to within about 2%, and the variations observed in Figs. 3(a) and 3(b) are a consequence of the projection.
[24] C. K. Harrison, Z. Cheng, S. Sethuraman, D. A. Huse, P. M. Chaikin, D. A. Vega, J. M. Sebastian, R. A. Register, and D. H. Adamson, Phys. Rev. E **66**, 011706 (2002).
[25] Although we also found that the data can be also well described by a power law, the resulting exponent is quite small ($\sim$0.04).
[26] A. P. Marencic, M. W. Wu, R. A. Register, and P. M. Chaikin, Macromolecules **40**, 7299 (2007).